7-1-2018

Experimental and Sensitivity Analysis of DMASP Cantilever Vibration Behavior Based on MCS Theory in the Moist Environment

M. H. Korayem
Iran University of Science and Technology

Byung I. Kim
Boise State University

A. H. Korayem
Boise State University

Experimental and sensitivity analysis of DMASP cantilever vibration behavior based on MCS theory in the moist environment

Abstract

A Micro-cantilever (MC) and a probe are two main components of the atomic force microscope (AFM). The dimensions of these components are in micro scales while their oscillation amplitude is on a nanometer scale. The present study intended to not only increase the accuracy of the simulation with regard to geometric discontinuities based on the Timoshenko Beam Model using the modified couple stress (MCS) theory but also increase the accuracy of the prediction of a system behavior by considering the effect hysteresis effect into the system vibration equations based on Bouc-Wen Model. Due to the lack of the experimental results for this kind of MCs, this paper is focused on the both experiment and simulation results by utilizing the DMASP micro cantilever. The vibration equations have been discretized based on the differential quadrature (DQ) model and solved using the Newmark algorithm and Laplace transforms in the free and forced vibration modes of AFM piezoelectric MC. The roughness of the surfaces affects the MC vibration behavior in the air medium. Therefore, surface roughness affecting van der Waals force has been considered in the air medium. Furthermore, the simulation results were compared with experimental results by performing experimental tests in the air medium with different moisture content. The experimental tests performed in the free vibration mode included frequency and time response and the forced mode sample surface topography and its effect on the MC vibration amplitude during the sample surface topography in different vibration modes. Moreover, the speed of equation solving was accelerated by performing sensitivity analysis based on the EFAST method as well as investigating the coupling effect of geometric and enforcement parameters on the amplitude and frequency of the MC and eliminating less effective parameters. The comparison of experimental results with theoretical results is indicative of the accuracy of MCS theory in the simulation.

Keywords: Atomic force microscopy, Piezoelectric micro cantilever, Timoshenko beam theory, Modified couple stress theory, Sensitivity analysis, Experiment, Air

1. introduction

The AFM has been known as one of the most effective measurement tools for measuring intermolecular forces, surface imaging and nanoparticles manipulation with a precision at the nanometer level. The use of classical continuum mechanics (CCM) is erroneous in system equations. Thus, providing modified models for increasing the accuracy of MC vibration equations along with performing experimental tests is greatly important. In this regard, three main works including classical continuum mechanics, modern continuum mechanics and sensitivity analysis have been carried out.

Concerning the modern continuum mechanics, Wang et al. extracted the single-layered Timoshenko beam equations based on the Hamilton's principle of couple stress theory [1]. Park and Gao modified the Euler Bernoulli beam equation with a rectangular cross section based on the couple stress theory [2]. Simsek proposed the Euler beam equation with a hollow-circular cross section with respect to the couple stress theory [3]. Asari et al. presented the piezoelectric MC using non-classical couple stress theory. They extracted MC equations for both Euler beam and Timoshenko beam with clamped-end (fixed-end) boundary conditions [4]. Reddy proposed Euler and Timoshenko beam equations using virtual methods and couple stress theory. He also considered axial force in the equations [5]. Wang et al. used the Timoshenko beam based on the couple stress theory for the FGM beam analysis [6].

Concerning AFM MC simulation, numerous researches have drawn on the methods of classical continuum mechanics. It should be noted that the use of continuum mechanics requires modification in case of micro and nanoscale dimensions. Since the AFM is examined in the air medium, the application of environmental forces to predict the MC vibration behavior is of utmost importance. Fung et al. considered the AFM MC vibrations with regard to the continuous piezoelectric layer and simulated a triangular end for MC [7]. Mahmoodi et al. studied piezoelectric AFM MC based on a multi-scale method for the natural frequency and obtained the natural frequency of the system for the first, second and third modes [8]. Mahmoodi and Jalili examined the piezoelectric MC regarding nonlinear flexural vibrations [9]. Wolf and Gottlieba studied silicon MC with integrated ZnO piezoelectric layer based on Lennard-Jones model for small displacements and used the multiscale-based perturbation method for solving the equations [10]. Korayem et al. analyzed the vibration motions of piezoelectric MC in non-contact mode and used numerical solutions to assess the nonlinear MC response in the vicinity of sample surface in the non-contact mode. They also investigated the effect of MC's angle, probe length and geometric dimensions of piezoelectric layer on the nonlinearity of the system's frequency response. On the other hand, they compared simulation results with experimental results in the absence of sample surface force to determine the accuracy of the non-uniform MC vibration model to simulate the piezoelectric MC vibration motion [11] and [12].

It is significantly necessary to investigate the effect of input parameters on the vibration behavior of the system in order to identify the effective parameters and eliminate the less effective parameters. In this regard, many studies have been done on the sensitivity analysis

of the AFM MC. Korayem and Damircheli simulated the AFM MC based on the Timoshenko beam theory and analyzed the frequency and amplitude sensitivity of the first four twisting modes for the variations of surface stiffness [13]. Son et al. analyzed the resonance frequency and the bending vibration sensitivity of the AFM MC. They calculated a closed loop equation for the sensitivity of vibration modes using the resonance frequency and MC stiffness [14]. Kovacs et al. analyzed the sensitivity of the piezo resistive and piezo capacity and performed sensitivity analysis for geometric parameters [15]. Lee et al. analyzed bending vibration sensitivity of a cracked AFM MC [16]. Korayem and Ghaderi studied the vibration behavior of piezoelectric MC in the air and a liquid medium. They also investigated the effect of MC geometric parameters on the MC behavior using Sobol sensitivity analysis [17].

The present study intended to simulate a comprehensive and precise model to evaluate the dynamic behavior of the system based on the MCS theory by considering the Timoshenko beam model, and used DQ method for discretizing the equation. In the simulation, the geometric discontinuities have been considered with regard to the presence of the piezoelectric layer bounded by two electrode layers as well as the variations of MC's cross section while connecting the probe to the MC. Furthermore, it considered the effect of environmental forces and sample surface forces including capillary, contact and van der Waals forces as the basis of the nanoscale surface topography, on the increase and decrease of MC vibration amplitude. In order to validate the accuracy of the proposed theory and the lack of the experimental results in this type of MC, its results were compared with experimental results which have been taken by DMASP microcantilever. Moreover, in order to select appropriate MC dimensions including the thickness, width and length of different MC layers i.e. silicon, piezoelectric and electrodes, the effect of dimensions on the sensitivity of vibration amplitude and frequency of the system was investigated using the EFAST sensitivity analysis.

2. piezoelectric MC dynamic modeling based on MCS theory

According to Figure (1), the proposed MC model is a four-layered clamped-free MC beam model including a ZnO piezoelectric layer, two Au electrodes and silicon clamped-free layers, with reduced probe cross section of the area. In this model, the MC's base was fixed while the piezoelectric layer considered as an actuator. In order to obtain the motion equations according to MCS theory, firstly the kinetic energy and secondly the potential energy of the system and external forces were calculated; subsequently, the equations and boundary conditions were extracted based on the Hamilton's principle.

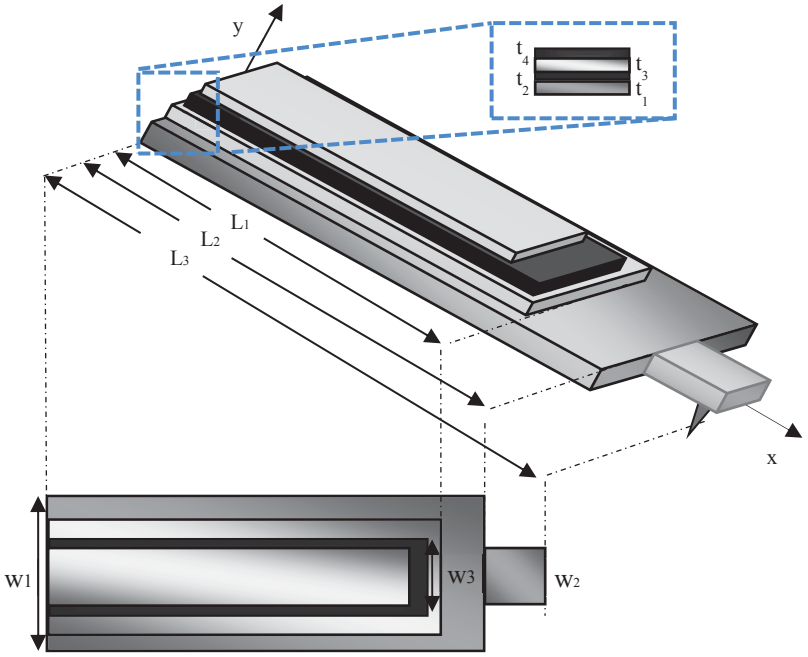

Fig.1. The AFM piezoelectric MC by considering geometric discontinuity.

In this model, the effect of tip mass was also considered. The equations and boundary conditions of non-uniform piezoelectric MC were obtained according to the reference [18] through Equation (1); where in this equation η, α, D, λ and μ are defined as $\eta = \frac{1}{4} l^2 A \mu$, $\alpha = (\lambda + 2\mu) I$, $D = \left[I_p - t_p \left(t_c + t_e - y_n + \frac{t_p}{2} \right)^2 \right]$, $\lambda = \frac{E\nu}{(1+\nu)(1-2\nu)}$ and $\mu = \frac{E}{2(1+\nu)}$ respectively.

$$\alpha \frac{\partial^2 \varphi}{\partial x^2} - \eta \left[\varphi + \frac{\partial w}{\partial x} \right] + \beta \left[\frac{\partial^2 \varphi}{\partial x^2} - \frac{\partial^3 w}{\partial x^3} \right] + D \left(\frac{e_1 e_5 + 2 e_1^2}{2\lambda_{33}} \right) \left(\frac{\partial^2 \varphi}{\partial x^2} + \frac{\partial^3 w}{\partial x^3} \right) \delta(x - L_1) = \rho I \frac{\partial^2 \varphi(x,t)}{\partial t^2}$$
$$\eta \left[\frac{\partial \varphi}{\partial x} + \frac{\partial^2 w}{\partial x^2} \right] + \beta \left[\frac{\partial^3 \varphi}{\partial x^3} - \frac{\partial^4 w}{\partial x^4} \right] - D \left(\frac{e_5 e_1}{4\lambda_{33}} \right) \frac{\partial^3 \varphi}{\partial x^3} \delta(x - L_1) + C \frac{\partial w}{\partial t} + F_{ts}(L_3, t) = \rho A \frac{\partial^2 w(x,t)}{\partial t^2} \quad (1)$$

And the boundary conditions were expressed in Equation (2)

$$BC:\begin{cases}\beta\left[\dfrac{\partial^2 w}{\partial x^2}-\dfrac{\partial\varphi}{\partial x}\right]-\alpha\dfrac{\partial\varphi}{\partial x}-D\left(\dfrac{e_1e_5+2e_1^{\,2}}{2\lambda_{33}}\right)\dfrac{\partial\varphi}{\partial x}\delta(x-L_1)-e_1\dfrac{z.V_H}{2t_p}\delta(x-L_1)\\ -D\left(\dfrac{e_5e_1}{4\lambda_{33}}\right)\dfrac{\partial^2 w}{\partial x^2}\delta(x-L_1)+\rho_{Ltip}M_{Ltip}\dfrac{\partial^2 w(L_3,t)}{\partial t^2}=0\Big|_{x=0}^{x=L}\\ OR\qquad \varphi=0\Big|_{x=0}^{x=L}\\ \beta\left[\dfrac{\partial^3 w}{\partial x^3}-\dfrac{\partial^2\varphi}{\partial x^2}\right]-\eta\left[\varphi+\dfrac{\partial w}{\partial x}\right]+D\left(\dfrac{e_5e_1}{4\lambda_{33}}\right)\dfrac{\partial^2\varphi}{\partial x^2}\delta(x-L_1)+\rho_{Ltip}I_{Ltip}\dfrac{\partial^2\varphi(L_3,t)}{\partial t^2}=0\Big|_{x=0}^{x=L}\\ OR\qquad w=0\Big|_{x=0}^{x=L}\\ \beta\left[\dfrac{\partial\varphi}{\partial x}-\dfrac{\partial^2 w}{\partial x^2}\right]-D\left(\dfrac{e_5e_1}{4\lambda_{33}}\right)\dfrac{\partial\varphi}{\partial x}\delta(x-L_1)=0\Big|_{x=0}^{x=L}\\ OR\qquad \dfrac{\partial w}{\partial x}=0\Big|_{x=0}^{x=L}\end{cases} \tag{2}$$

Also, the constant coefficients associated with each MC segment are defined in Table (1).

Table. 1. The constant coefficient of each MC section

Beam section	α	η	ρI	β	ρA
$0 < x < L_1$	$\sum_{j=1}^{4}\alpha_j$	$\sum_{j=1}^{4}\eta_j$	$\sum_{j=1}^{4}\rho_j I_j$	$\sum_{j=1}^{4}\beta_j$	$\sum_{j=1}^{4}\rho_j A_j$
$L_1 < x < L_2$	α_c	η_c	$\rho_c I_c$	β_c	$\rho_c A_c$
$L_2 < x < L_3$	α_{tip}	η_{tip}	$\rho_{tip} I_{tip}$	β_{tip}	$\rho_{tip} A_{tip}$

In order to apply the hysteresis effect, Equation (3) was used based on Bouc-Wen Model.

$$\begin{aligned} V_H(t) &= \alpha k V(t)+(1-\alpha)Dkz(t)\\ \dot{z} &= D^{-1}\left(A\frac{\partial V(t)}{\partial t}-\beta\left|\frac{\partial V(t)}{\partial t}\right||z|^{n-1}z-\gamma\frac{\partial V(t)}{\partial t}|z|^{n}\right)\end{aligned} \tag{3}$$

Where V(t) is the input voltage and Z(t) is hysteresis displacement. The parameters of α, A, β, γ *and* n play a crucial role in creating and controlling the dimensions and shape of the hysteresis loop. The values of the parameters were derived from the reference (20). The vibration equations of the system have been discretized based on DQ model and solved using the Newmark algorithm and Laplace transforms. By discretizing the equations based on DQ method, the vibration equations of the systems were transformed to the discretized equation (4).

$$\begin{aligned} &M_I\ddot{q}_I+K_{II}q_I+K_{BC}q_{BC}+c_I\dot{q}_I=0\\ &q_{BC}=\left[K_{BCBC}\right]^{-1}.f-\left[K_{BCBC}\right]^{-1}.K_{BCI}.q_I\end{aligned} \tag{4}$$

By combining both equations above, the final equation discretized based on the DQ is presented as Equation (5).

$$M_I \ddot{q}_I + \left[K_{II} - K_{BC}\left[K_{BCBC}\right]^{-1}.K_{BCI} \right] q_I + c_I \dot{q}_I = K_{BC}\left[K_{BCBC}\right]^{-1}.f \tag{5}$$

In Equation (5), the indexes of BC, I. II. IBC, BCI and BCBC respectively signify boundary points, internal points, internal node coefficients of stiffness matrix, boundary node coefficients of stiffness matrix, internal node coefficients of boundary conditions matrix and boundary node coefficients of the boundary conditions matrix. In order to calculate the frequency response based on Laplace transforms, the frequency response of the system was obtained through Equation (6).

$$\begin{aligned} L\{q_I(\omega)\} &= \frac{L\{F\}}{-\omega^2.M + \bar{K} + j\omega.C} \\ L\{q_{BC}(\omega)\} &= \left[K_{BCBC}\right]^{-1}.\mathrm{L}\{f\} - \left[K_{BCBC}\right]^{-1}.KK_{BCI}.L\{q_I(\omega)\} \\ \bar{K} &= K_{II} - K_{BC}\left[K_{BCBC}\right]^{-1}.K_{BCI} \\ F &= K_{BC}\left[K_{BCBC}\right]^{-1}.f \end{aligned} \tag{6}$$

Moreover, the time response of the system can be obtained through Equation (7) based on the Newmark algorithm.

$$q_I(t+\Delta t) = \left[\tilde{K}\right]^{-1}\left\{F_{eff}(t+\Delta t)\right\} \tag{7}$$

$$\left[\tilde{K}\right] = \frac{4}{\Delta t^2}[M] + \frac{2}{\Delta t}[C] + \left[\bar{K}\right]$$

$$F_{eff}(t+\Delta t) = F(t+\Delta t) + [M]\left(\ddot{q}_I(t) + \frac{4}{\Delta t}\dot{q}_I(t) + \frac{4}{\Delta t^2}q_I(t)\right)$$

$$+[C_I]\left(\dot{q}_I(t) + \frac{2}{\Delta t}q_I(t)\right)$$

3. Tip-Sample Force in the Vicinity of sample surface

AFM consists of an elastic Microcantilever that is influenced by the complex interactions between probe and sample surface. The probe-sample interaction includes van der Waals attractive forces, capillary forces caused by liquid layer and repulsive forces representing the onset of contact, which has been symbolized as $F_{ts}(L_3, t)$ in Equation (1). At distances away from the surface, the dominant force is the attractive force. The attractive force can be described by van der Waals force. When the probe is sufficiently placed in the vicinity of the sample surface, the repulsive force will be dominant. In addition to the repulsive force, there is also a van der Waals force that can be described by adhesive force. The tip-sample force changes over time. The tip-sample force is a van der Waals attractive force when the probe or

cantilever approach the object before reaching the distance of d_{on} $(d_{ts} > d_{on})$.

$$F_{ts}(L_3,t) = \begin{cases} F_{vdw}(d_{ts}) & d_{ts} > d_{on} \\ F_{vdw}(d_{ts}) + F_{cap}(d_{ts}) & a_0 < d_{ts} < d_{on} \\ F_{vdw}(a_0) + F_{cap}(a_0) + F_{adh}(d_{ts} - a_0) & d_{ts} < a_0 \end{cases} \quad (8)$$

Once the probe or MC reaches the distance of $d_{on}(a_0 < d_{ts} < d_{on})$, the capillary force $(F_{cap})$is added. Since the capillary force is stronger than van der Waals force, it immediately leads F_{ts} to negative values. In the molecular distance of $a_0(d_{ts} < a_0)$, the strong repulsive contact force (F_{DMT}) operates. The van der Waals force is constant when the probe is located in the distance of $d_{ts} \leq a_0$ from the surface which equates to its value in $d_{ts} = a_0$.
All the existing surfaces in nature have roughness. This roughness is more visible in nanometer dimensions and subsequently affects the vibration behavior of the AFM MC and the quality of sample surface imaging. This impact is due to the significant reduction in the adhesion between the surfaces or between a particle and a surface. The reason for the reduction of the contact surface is the porosity of the surface with respect to the surface roughness models that affect the van der Waals force.

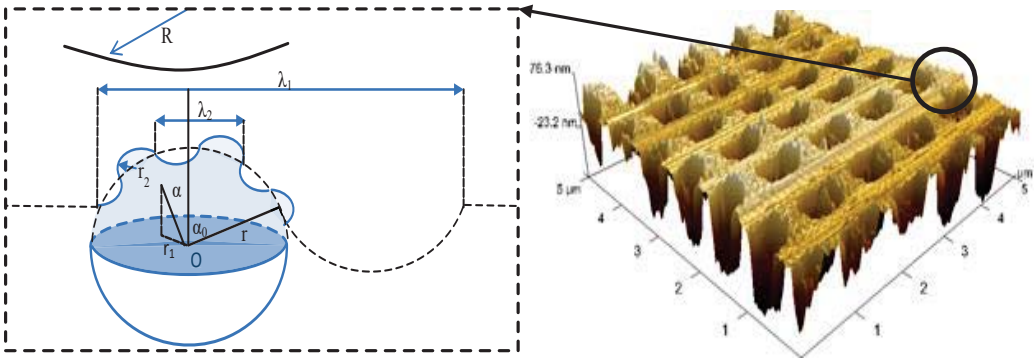

Fig. 2. Description of the Roughness based on Katainen Model

In Equation (9), the first, second and third terms are related to the interaction of the particle with n-th secondary dump and bump, primary dump and bump and mean plate [19].

$$F_{vdw-kumar} = \frac{A_H R}{6H_0^2}\left[n\frac{1}{1+\left(\frac{58Rrms_2}{\lambda_2^2}\right)} + \frac{1}{\left(1-\frac{58Rrms_1}{\lambda_1^2}\right)\left(1+\frac{1.82rms_2}{H_0}\right)^2} + \frac{H_0^2}{(H_0+1.82(rms_1+rms_2))^2}\right] \quad (9)$$

In the denominator of the second term, the negative sign is due to the interaction of the particle with hollowness between the primary dumps and bumps. The prerequisite for the validity of this model is that the $\lambda_1 > \sqrt{58Rrms_1}$ and the critical tip-to-tip distances of primary dump and bumps are obtained through $\lambda_{critical} = \sqrt{58Rrms_1}$, where A_H is the Hamaker Constant, R is the radius of the probe tip curvature and d is the tip-sample distance. The

Hamaker constant is calculated through Equation (10). The indices of 2, 1 and 3 signify first body, fluid interface, and second body respectively.

$$A_H = \frac{3}{4}K_B T\left[\frac{\varepsilon_1-\varepsilon_3}{\varepsilon_1+\varepsilon_3}\right]\left[\frac{\varepsilon_2-\varepsilon_3}{\varepsilon_2+\varepsilon_3}\right]+\frac{3}{8}\frac{h\nu_e}{\sqrt{2}}\frac{\left(n_1^2-n_3^2\right)\left(n_2^2-n_3^2\right)}{\sqrt{n_1^2+n_3^2}\sqrt{n_2^2+n_3^2}\left(\sqrt{n_1^2+n_3^2}+\sqrt{n_2^2+n_3^2}\right)} \tag{10}$$

The Hamaker constant has a direct impact on interatomic forces. Therefore, the accurate calculation of the Hamaker constant is effective in surface topography. The Hamaker constant between two surfaces is dependent on the material of the first body, fluid interface and the material of the second body. Besides, the surface energy is calculated through equation $\gamma_s = \frac{A_H}{24\pi D_0^2}$.

In addition to the van der Waals force, the capillary force affects the vibration amplitude of the system. This force occurs due to the collision of thin water layers with thickness h that have been accumulated on the probe tip and sample surface. In environmental conditions, a water layer of hydrocarbon layer is often placed between the probe tip and the sample surface. The capillary meniscus can grow until the rate of evaporation and condensation is in a state of equilibrium with the environment. The capillary meniscus produces a great surface tension between the molecules at a distance away from the molecular distance. This effect is known as Laplace pressure that draws the probe tip to the sample surface and is known as a capillary effect or capillary action in practice. The pressure difference between the joint surfaces is due to the capillary condensation. This phenomenon occurs when the cracks, porosity of the surface is equal to the Kelvin radius [20]. If the probe geometry is considered as a sphere and plate, this force is calculated through Equation (11).

$$F_{cap}(d_{ts}) = 4\pi\gamma_w\ cR\left(1-\frac{d_{ts}}{\sqrt{\frac{V}{\pi R}+{d_{ts}}^2}}\right) \tag{11}$$

Where

$$V = \pi R\left(4r^2c^2-{d_{ts}}^2\right) \quad ; \quad c = \frac{\cos(\theta_1+\beta)+\cos\theta_2}{2} \tag{12}$$

In Equation (12), θ_1 is the angle between probe and meniscus, θ_2 is the angle between the sample surface and meniscus and β is the angle between the meniscus and the center of the sphere that is calculated through Equation (13).

$$\beta = Arc\sin\left[\frac{x_1}{R_{tip}}\right] \tag{13}$$

Figure (3) displays the variation of the radius of the meniscus curvature in terms of probe tip-sample distance. As illustrated, with the proximity of the robe tip to the sample surface, the center of the meniscus curve increased in comparison to the center of the probe symmetry.

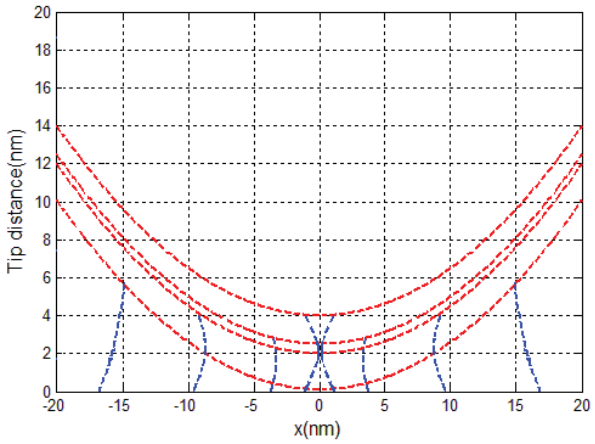

Fig. 3. Variation of the meniscus by Approaching the Probe Tip to the Sample Surface

The contact force is defined as the collision of two objects or bodies such as probe tip and sample surface in the AFM. It is used to estimate the real reactions of two surfaces with different curvature radii, where E_1 and E_2 are the modulus of elasticity and V_1 and V_2 are the Poisson coefficients of two surfaces in contact with each other.

$$F = \frac{4\pi q_k}{3\left(\frac{1-\upsilon_1^2}{E_1}+\frac{1-\upsilon_2^2}{E_2}\right)\sqrt{A+B}}\alpha^{\frac{3}{2}} \tag{14}$$

4. DMASP experimental and theoretical results

The intended AFM was used to perform the experimental tests such as Multimode-IIIA AFM. One of the characteristics of this model is the use of a different scanner, controller and probes in different operation modes. Figure (4) illustrates a representation of the intended system.

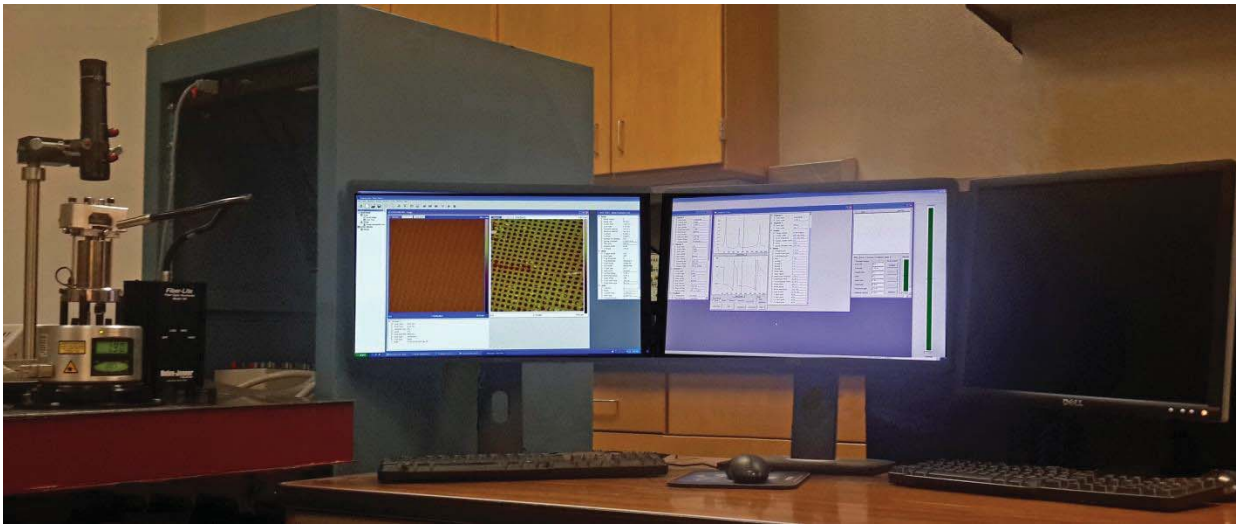

Fig. 4. AFM Multi mode system by utilizing Nanoscope IIIA controller

Figure (5) shows the MM-SSM microscope with 3 pins on its scanner by means of which the laser is positioned at the end of the cantilever and photodiode. There are two tension springs on each side of the scanner that are used to hold the scanner. The probe-sample distance can be adjusted manually and automatically by means of the screws at the end of the scanner. The photodiode has four parts: parts A and B measure the vertical displacement and parts C and D measures the horizontal MC displacement. The numbers on AFM screen display the instantaneous amplitude and change of the photodiode signal. Moreover, the other system inputs are used for measuring and imaging the properties of the sample using Nanoscope software and Nanoscope iiia controller.

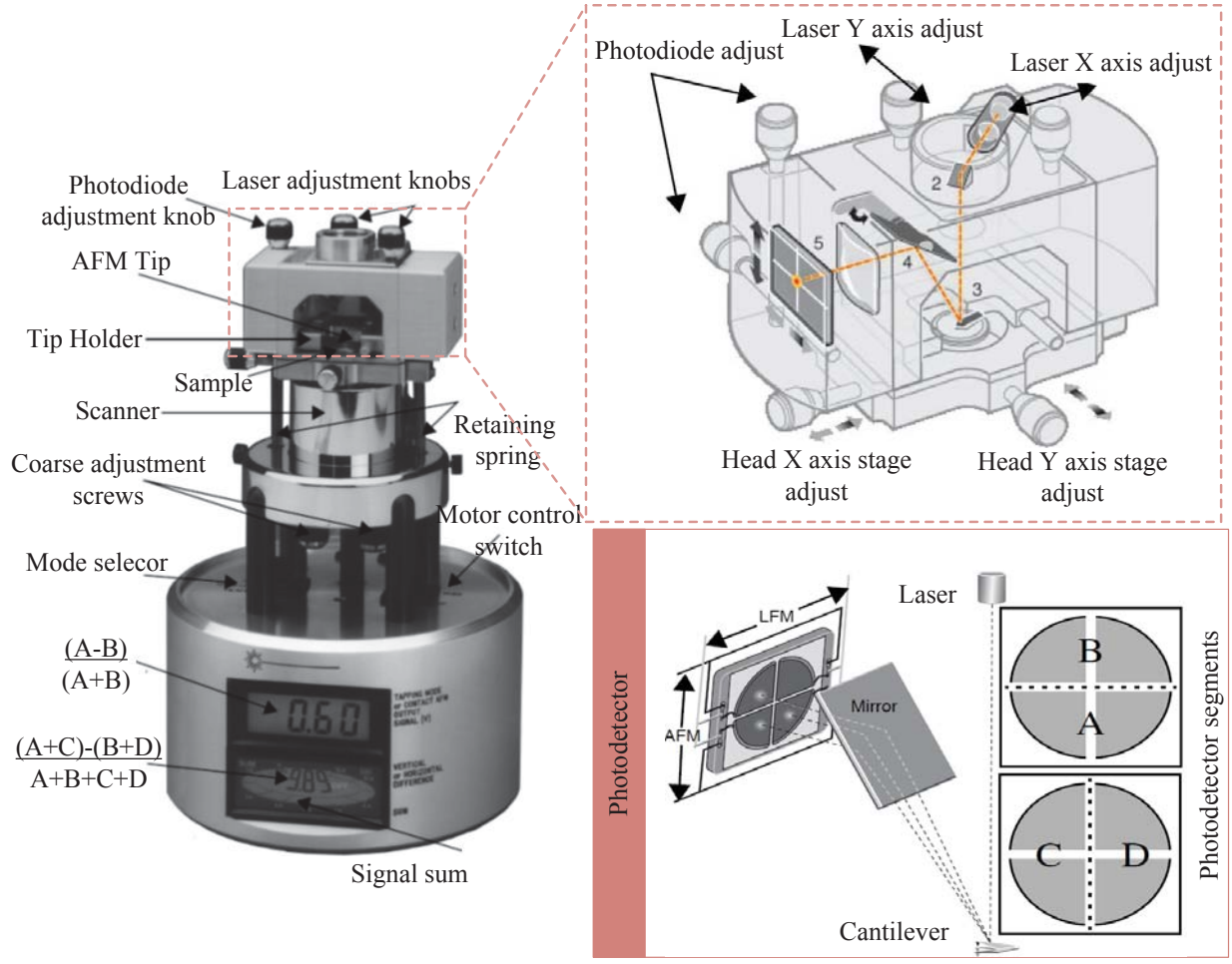

Fig. 5. different part of the Multi mode spm and photodetector

4.1. piezoelectric MC frequency response

The intended piezoelectric MC used in experimental tests is DMASP micro cantilever which is made by Veeco Company. This MC consists of a ZnO piezoelectric layer with a thickness of 3.5 micrometers along with two Au electrodes with a thickness of 0.25 micrometer and the sensitivity coefficient converts the output signal from the voltage to nanometer by providing

the conversion sensitivity coefficient of 20nm/v. The detailed specifications of MC are presented in Table (2).

Table. 2. DMASP micro cantilever geometric detail

Parameter	Material	L	W	T	P	E
Unit	-	(μm)	(μm)	(μm)	(kg/m3)	(Gpa)
Cantilever	Si	351	258	3.5	2330	105
Lower electrod	Au	335	190	0.25	19300	78
Piezoelectric layer	ZnO	335	190	3.5	6390	104
Upper electrode	Au	335	190	0.25	19300	78
Tip	Si	150	70	3.5	2330	105

According to Figure (6), the first, second and third natural frequency of the system were estimated as 56.28 kHz, 200 kHz and 421 kHz respectively by applying a voltage of 30 millivolts to the MC and using the sensitivity coefficient of 20 nm/v. Moreover, by simulating the MC according to the specifications of Table (2), the first three natural frequencies are 56.23 kHz, 201.3 kHz and 423 kHz respectively with an error rate of %0.09, %0.95 and %0.47 respectively.

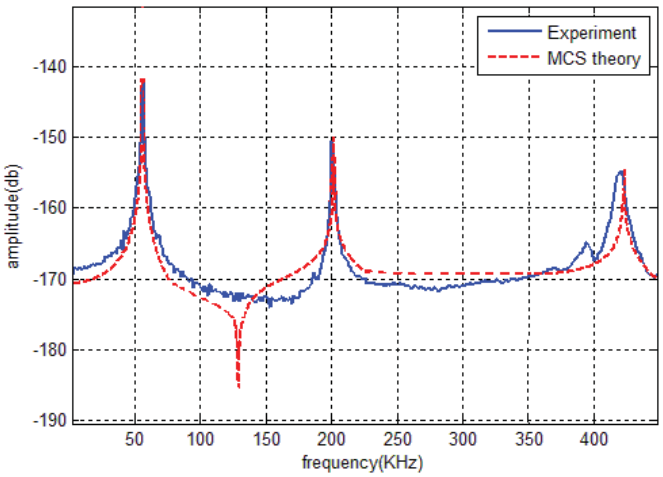

Fig. 6. Comparison between theoretical and experimental frequency response by using the DMSAP cantilever

Figure (7) shows the reduction of the first to third natural frequencies of AFM piezoelectric MC by the approaching to the equilibrium distance of the system. This frequency reduction is accompanied by a reduction in the MC vibration amplitude. The reduction contributes to the presence of probe-sample forces including van der Waals, capillary and contact forces that have a greater impact on the reduction of the system's frequency and amplitude by decreasing the equilibrium distance.

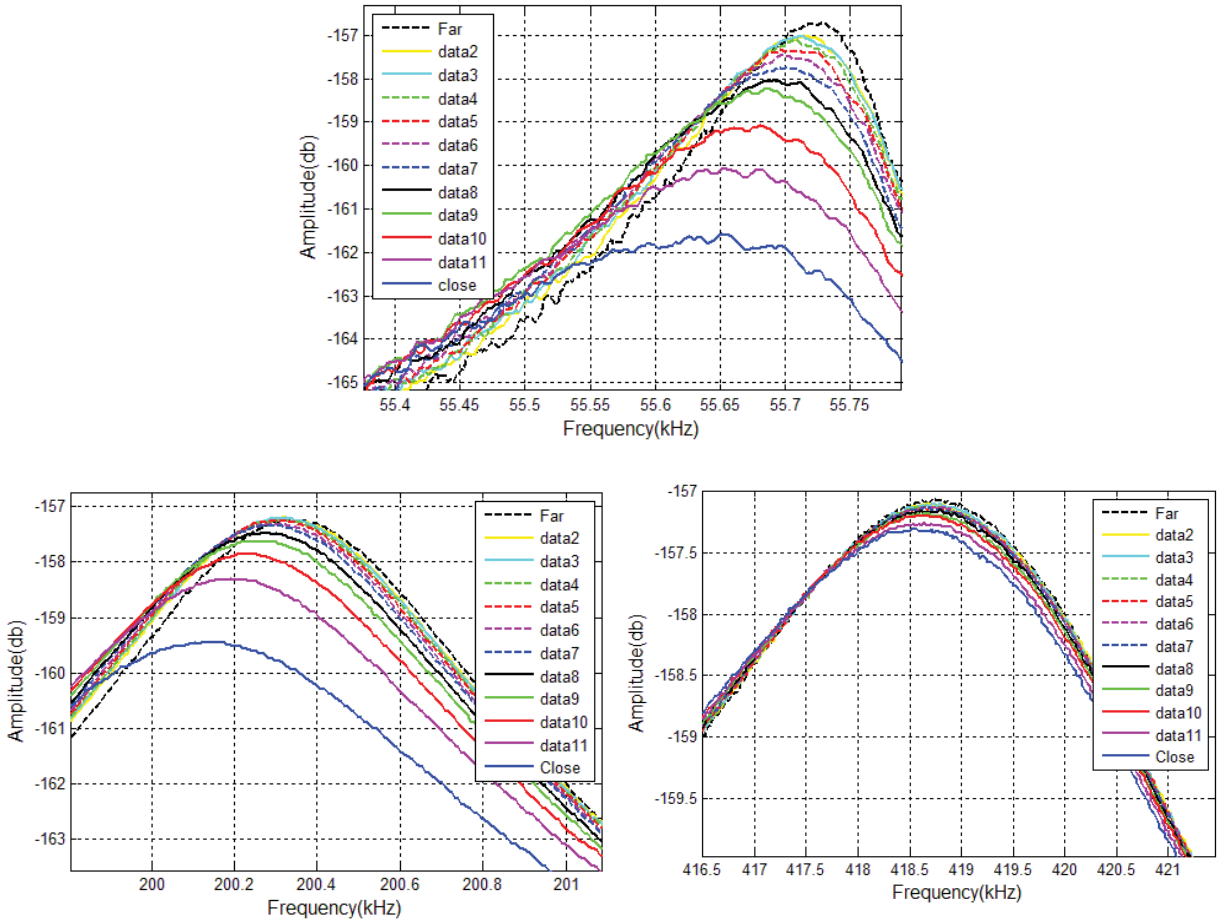

Fig.7. Variations of the First to Third Natural Frequencies of MC based on the Reduction of Tip-sample distance

4.2. DMASP piezoelectric MC time response

The AFM piezoelectric MC is simulated by applying a sinusoidal voltage in the amplitude mode. In most cases, the MC is simulated at a frequency close to the natural frequency of the system due to the high voltage intolerance by the piezoelectric layer. Therefore, an appropriate vibration amplitude is created by simulating the MC in the vicinity of the resonance frequency with a lower voltage. Furthermore, the maximum applicable voltage is 5V because of the voltage tolerance limit for the piezoelectric layer. With respect to the MC vibration equation based on the MCS theory and the Timoshenko beam assumptions, the equations were discretized according to the DQ method and solved using Laplace transforms and the Newmark algorithm. Regarding the comparison of the first three vibration modes of the system, as shown in Figure (8), the theoretical results have a good agreement with experimental results.

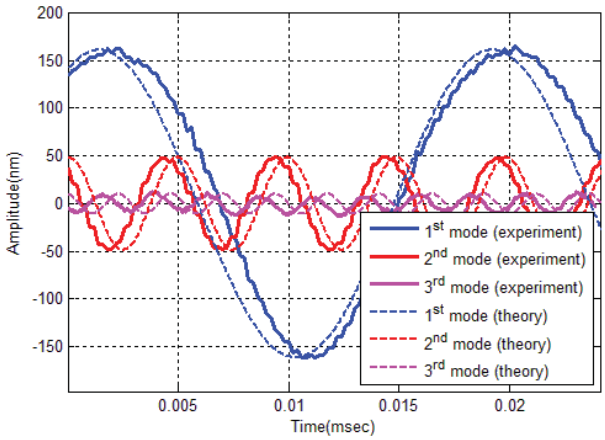

Fig. 8. First three vibration amplitude of piezoelectric microcantilever

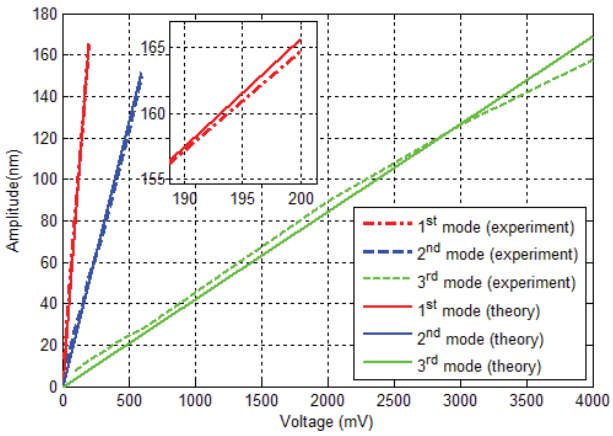

Fig. 9. variation of MC vibration amplitude based on the voltage increase for first three vibration mode

Under same conditions and applying 200 mv voltage, the vibration amplitude was equal to 161.9 nm, 47.91 nm and 10.3 nm respectively for the first to third modes while it was 161nm, 48.5 nm and 10.3 nm according to experimental results. Moreover, according to Figure (8) the variations of MC vibration amplitude based on the voltage increase for the first three vibration modes of the system, the amplitude increase was linear. According to Figure (9), under the same environmental conditions, the system had the higher energy to achieve equal vibration amplitudes in higher vibration modes than lower vibration modes.

4.2.1.Surface topography by DMASP Microcantilever

This section provides sample surface topography in different operating modes by the DMASP Microcantilever. According to Figure (10), sample surface topography had a better quality and higher accuracy in the third mode than the first two modes.

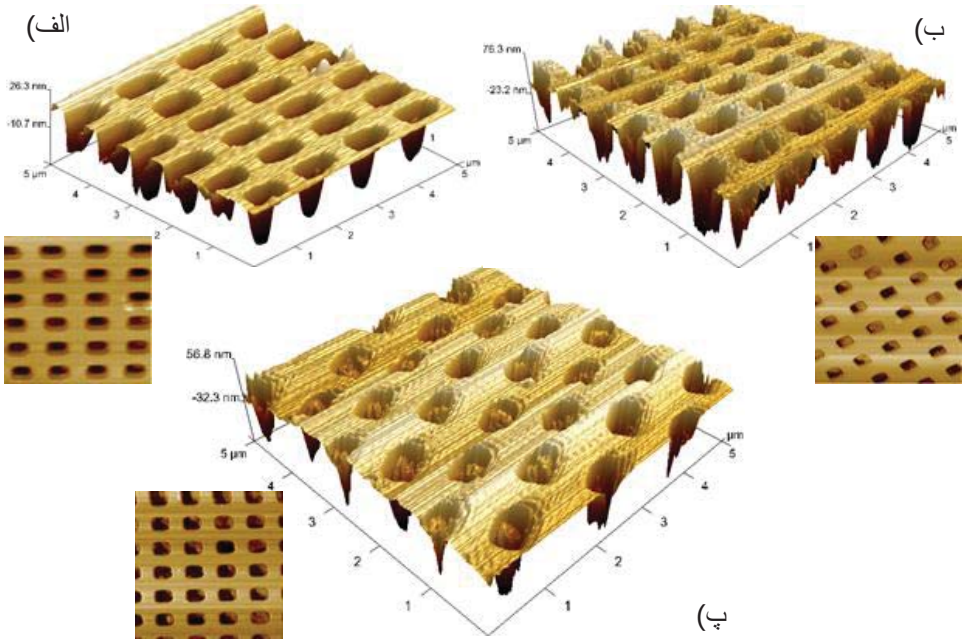

Fig. 10. 2D surface topography, a) first mode, b) second mode, c) third mode

Based on the sample surface topography, the available images have many 2D lines that demonstrate surface oscillations in details. These lines can be in different directions. For instance, the intended directions for this section are shown as the blue arrow (Figure 11).

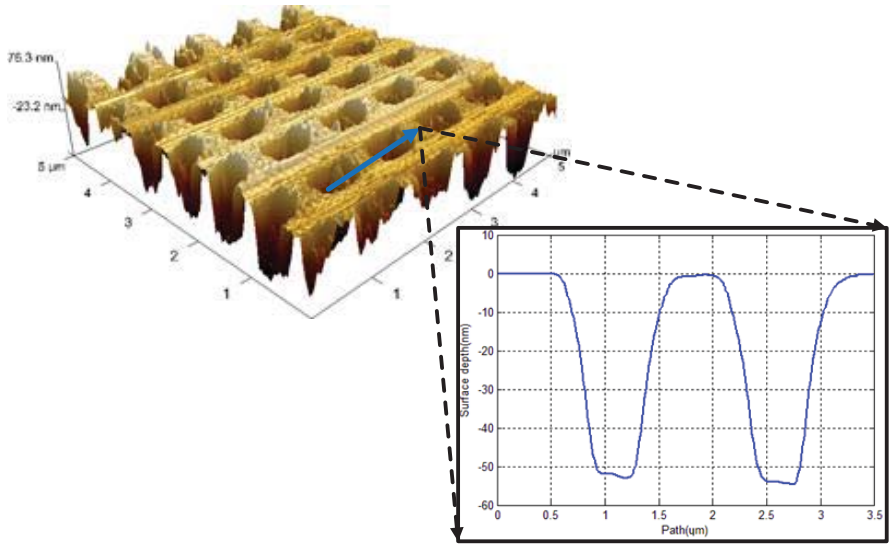

Fig. 11. Line analysis in the arrow direction

A noted earlier, the sample surface topography of the first three vibration modes of the system has been done according to Figure (11). Since the theoretical results were dependent on MC vibration without using a controller to achieve a time response, the control loop is inactive for attaining a time response and the output signal was measured and recorded by an Oscilloscope and SAM device manufactured by VEECO company.

Figure (12) displays the time response of DMASP piezoelectric Microcantilever in the first three vibration modes. As illustrated, the MC time response is more accurate followed sample surface roughness as the operating mode increased because the number and speed of data collection from the sample surface increased. Comparing the theoretical and experimental results on the first vibration modes in the air medium according to Figure (12), the time delay decreased in the first two modes by increasing the vibration mode while the time delay in the third vibration mode can be neglected. Therefore, higher vibration modes are recommended to attain more accurate and high quality sample surface topography. Besides, the difference between theoretical and experimental results indicates the existence of interatomic forces in addition to van der Waals, capillary and contact forces.

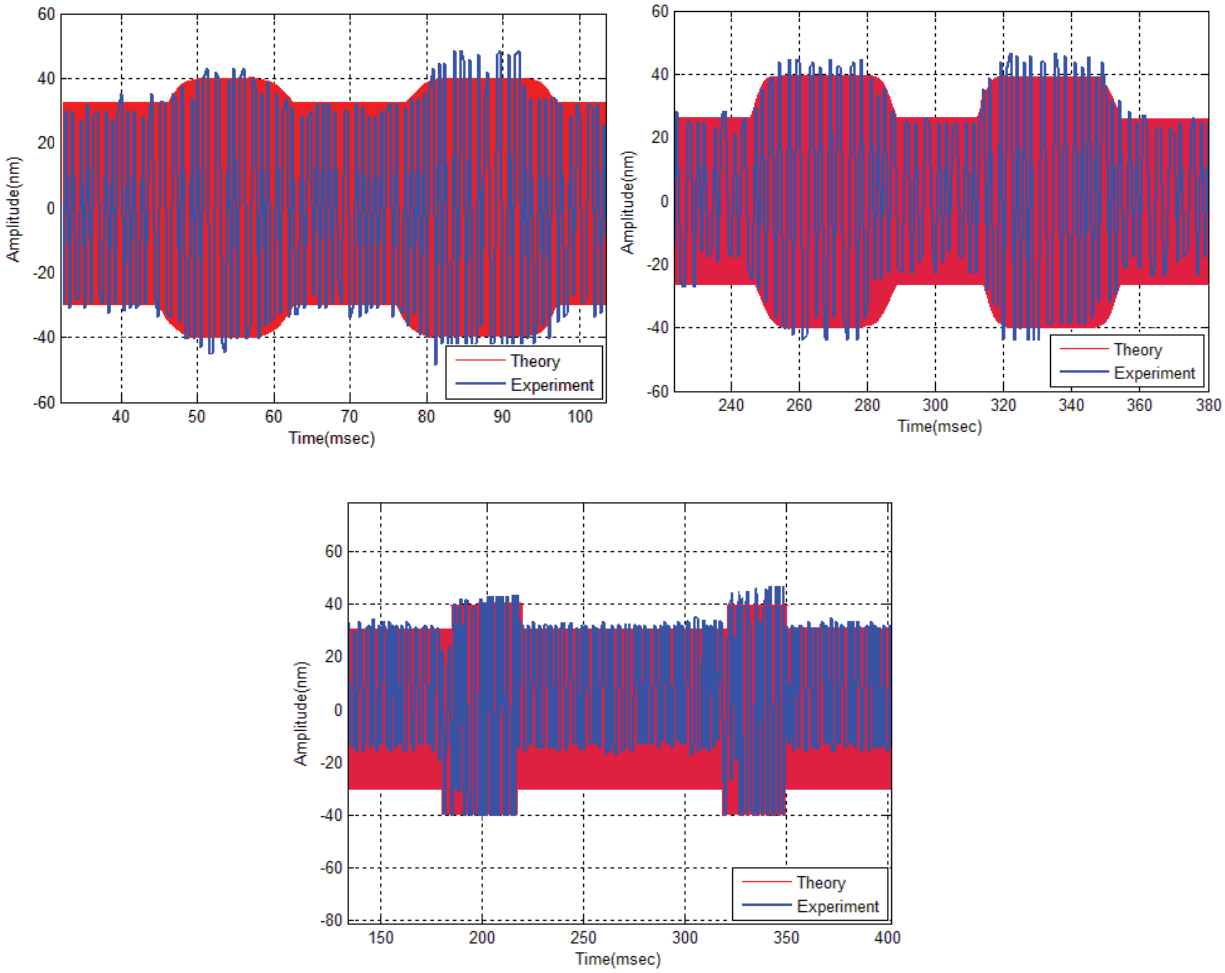

Fig. 12. DMASP micro cantilever time response while crossing the surface roughness, a) First mode. b) Second mode. c) Third mode.

4.3.Humidity

Figure (13) shows how to control the humidity percentage of the environment. From right to left, the compressed air through directing pumps and pipes is divided into the dry and humid

air by a flowmeter. The dry air flows directly into the compartments and the humid air is controlled by passing to the water pool and then enters the compartment. The experiment is made possible by providing appropriate environmental conditions and measuring the humidity percentage of the air by means of sensors.

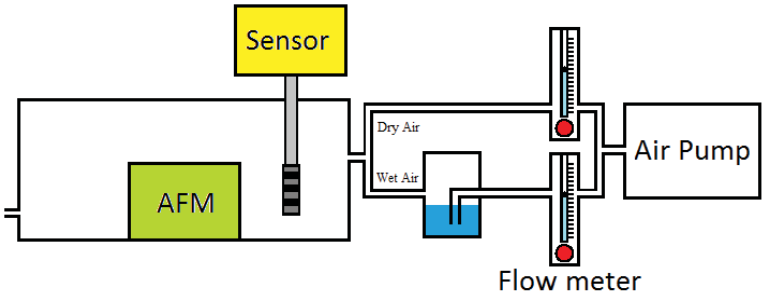

Fig. 13. Controlling the environmental humidity percentage

The air humidity affects the vibration amplitude and frequency of the system when the MC is near to or far from the surface. According to Figure (14), when the vibration amplitude and natural frequency of the MC are influenced by changing the damping factor when the MC is far from the sample surface and by changing the capillary force when the MC is near to the sample surface.

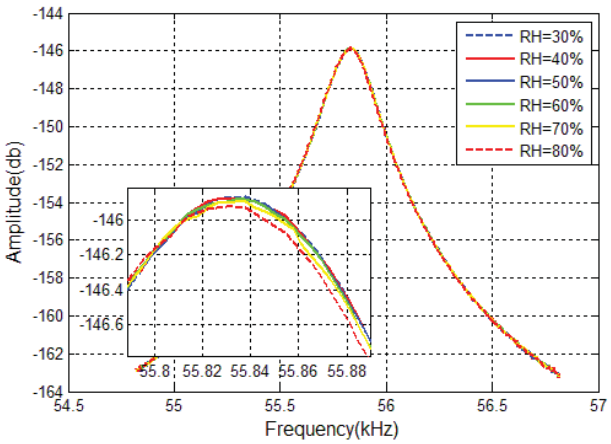

Fig. 15. Frequency response in different humidity percentage

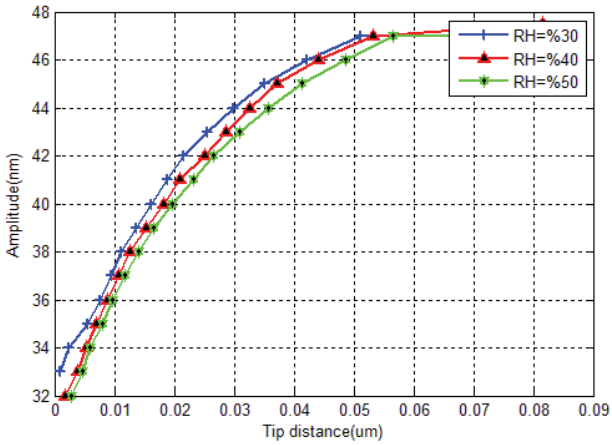

Fig 14. Variations of MC Amplitude based on Equilibrium Distance Variations in Different humidity percentage

Figure (15) shows the frequency response of the MC in different moisture contents ranging from 30 to 80 degrees. As illustrated, the vibration amplitude decreased by increasing the air moisture content and damping coefficient.

5. DMASP micro cantilever sensitivity analysis

The sensitivity analysis is used to remove the parameters that are less effective in the model and can be removed. They can also be used to define an optimal area for the parameters. The other goal of sensitivity analysis is finding areas in the entire input range for achieving the maximum changes in the output of the model for each parameter. If some input parameters are dependent on each other or are coupled, it won't be easy to find the effect of the parameters in the answer to the problems because most parameters are interconnected and cannot be separable. On the other hand, reducing the number of parameters to simplify the model is another goal of sensitivity analysis. In this case, the number of parameters can be reduced by finding the sensitive and non-sensitive parameters and neglecting the non-sensitive values constant. This is mostly used in the models where the numbers of parameters are numerous. This can reduce the number of equations and calculations in the models with abundant coupled equations.

Figure (15) shows the effect of all parameters on the MC frequency and time response in different operating environments including air, liquid and vacuum media. These parameters are classified into two general groups of environmental and geometric parameters. The geometric parameters are related to the MC geometry comprising 9 parameters of the length, width and thickness of the MC. The environmental parameters include parameters that generate probe-sample forces. Figure (16) displays the general process of identifying these parameters.

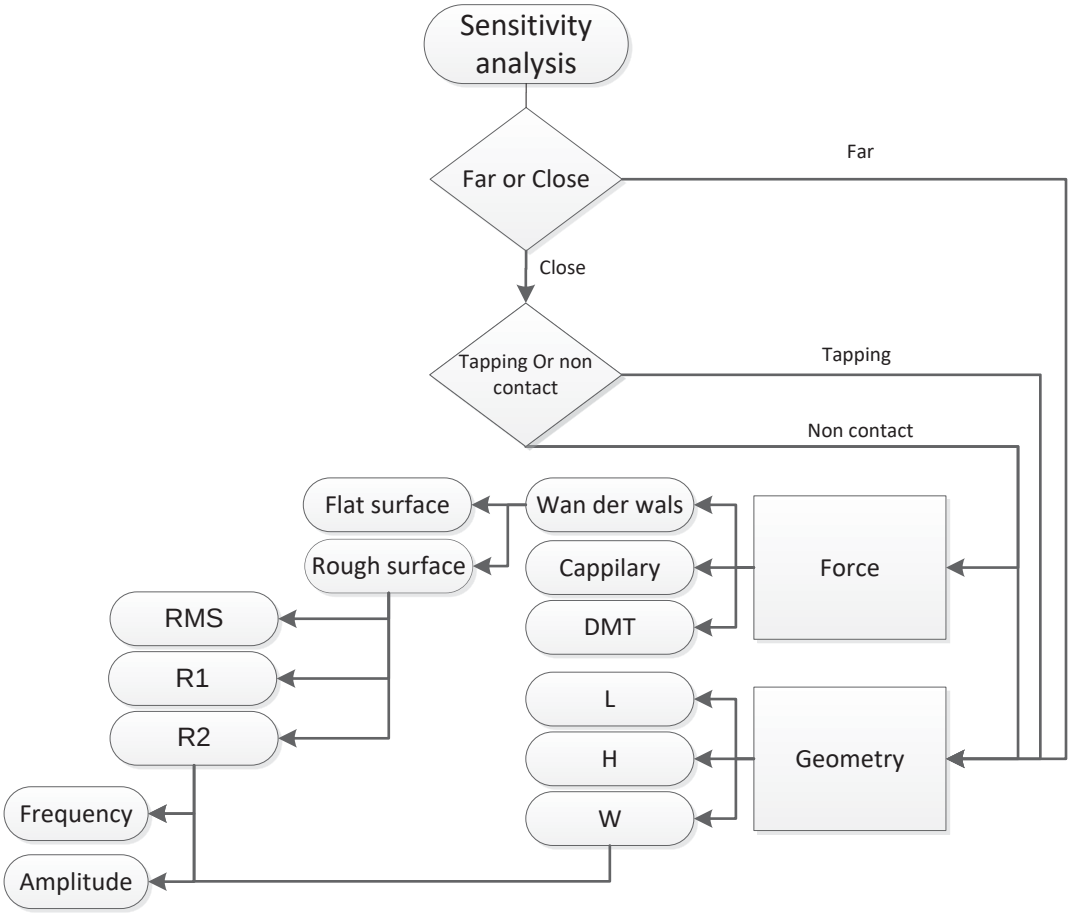

Fig. 16. Sensitivity analysis parameter flowchart

6. Effect of geometric parameter on the MC amplitude and frequency response

To this end, the present study investigated the effect of 9 geometric parameters of MC, including the length of the first part (L_1), length of the middle part of the MC (L_1-L_2), length of the tip (L_2-L_3), as well as MC thickness and width, piezoelectric layers and electrodes, on the first three natural frequencies and on the MC vibration amplitude. According to Figure (17), the increase of MC length decreased the MC frequency because the natural frequency decreases due to the increase of the MC length and having a reverse relation with the MC length.

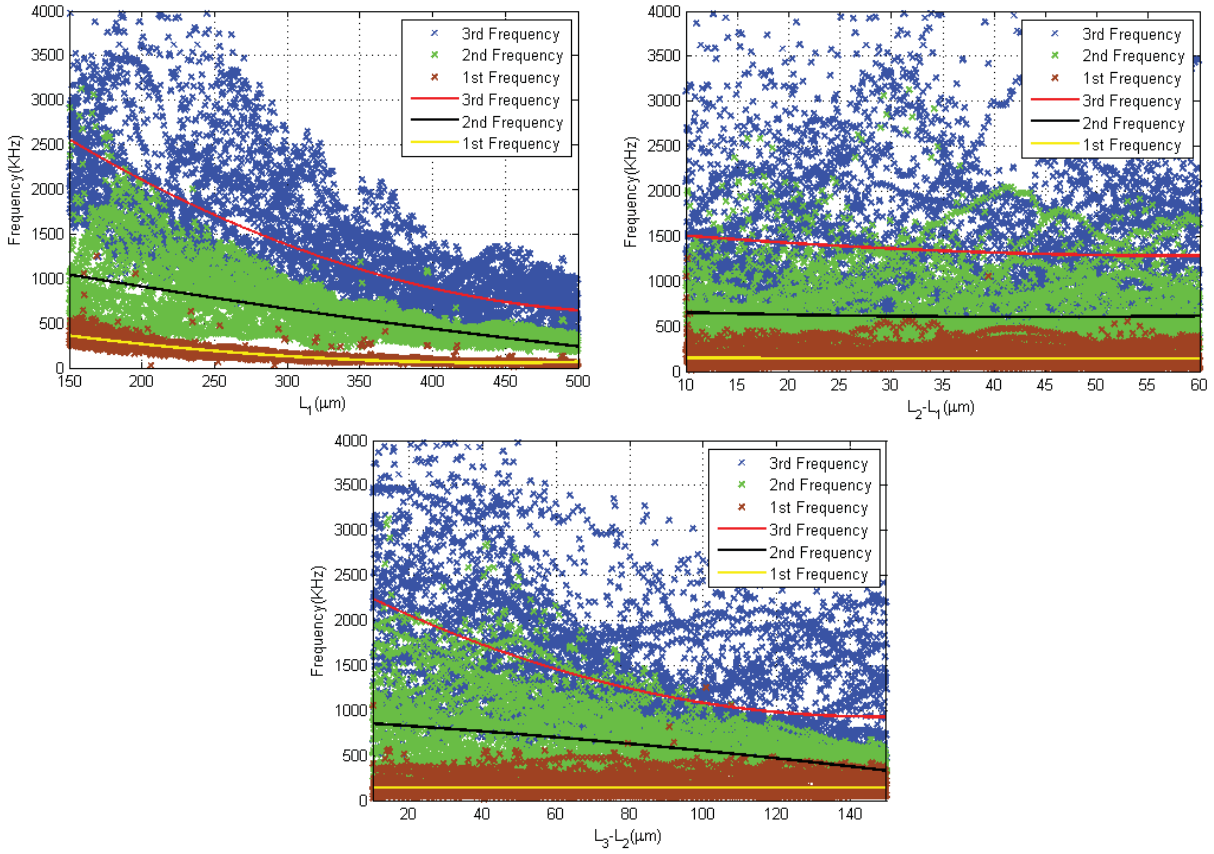

Fig. 17. Effect of MC length on the first three natural frequency

Figure (18) shows the effect of the MC thickness (H_1), piezoelectric (H_2) and electrodes (H_3) on the first three MC natural frequencies. Since the MC stiffness increased by increasing the thickness of each layer, the increased thickness will result in higher natural frequency. With regard to the results, the MC thickness and piezoelectric layer imposed more variations on the natural frequency due to their wideness while the electrode had a less significant effect on the MC stiffness due to less wideness and thickness. Therefore, increasing their thickness does not cause great variations in the natural frequency. The results also indicate that thickness of the piezoelectric layer had a greater effect on the first frequency than the other layers. This is while the slope of the graph is greater for MC thickness in higher modes.

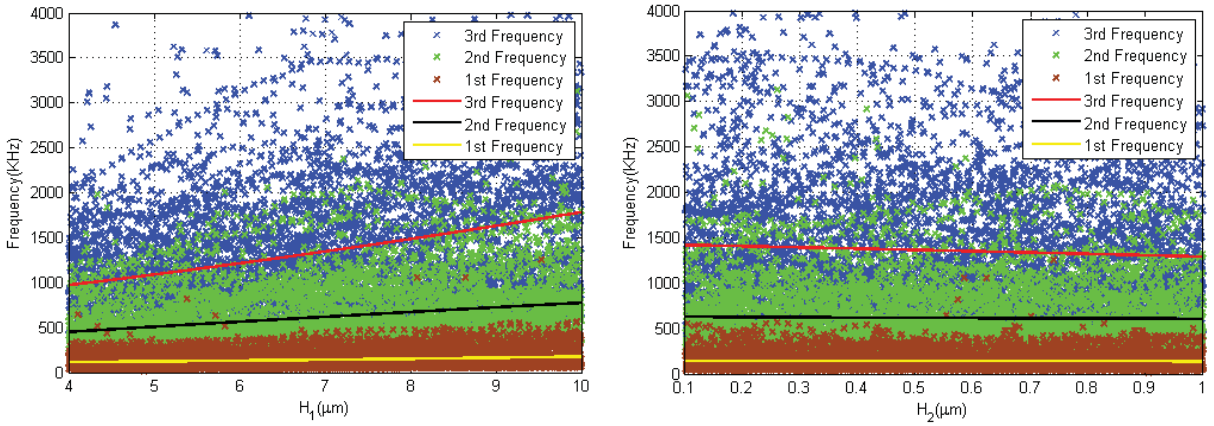

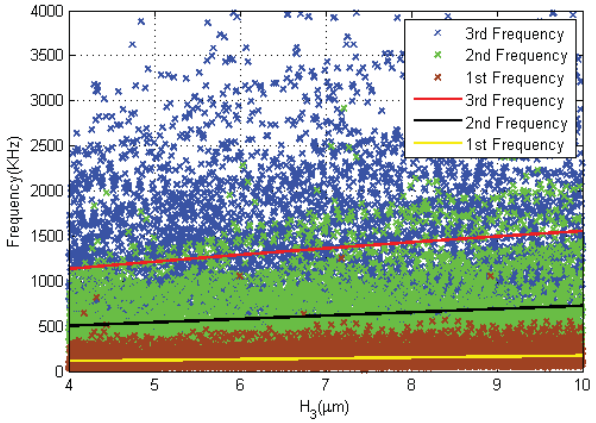

Fig. 18. Effect of MC thickness on the first three natural frequency

According to Figure (19), the increase in the MC width caused a slight change in the increase or decrease of the MC's natural frequency because the natural frequency increases due to the increase of the cross section and inertia moment by increasing the MC width.

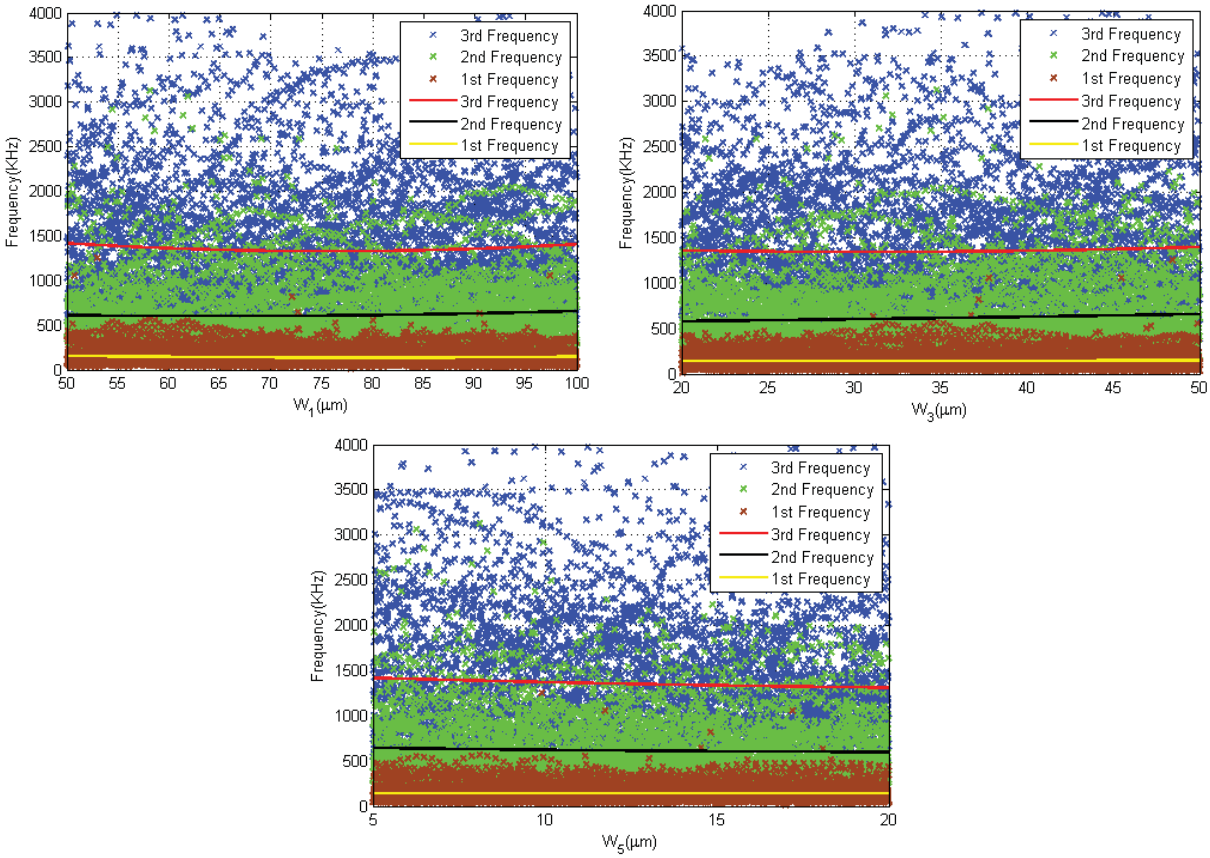

Fig. 19. Effect of the MC width on the MC first three natural frequency

The effect of input parameters on output parameters is investigated in sensitivity analysis. The advantage of this method is investigating the general effect of the input parameters on the output. In other words, the parameters are analyzed as a couple. In this regard, the effect of parameters are evaluated two by two or three by three etc. The results of investigating the effect of geometric parameters on the first three natural frequencies are presented in Figure (20). According to this figure, the length of the first part of the MC, signified by L_1, had the

maximum effect on the natural frequencies. The width of electrodes had the minimum effect on the natural frequency variations of the system.

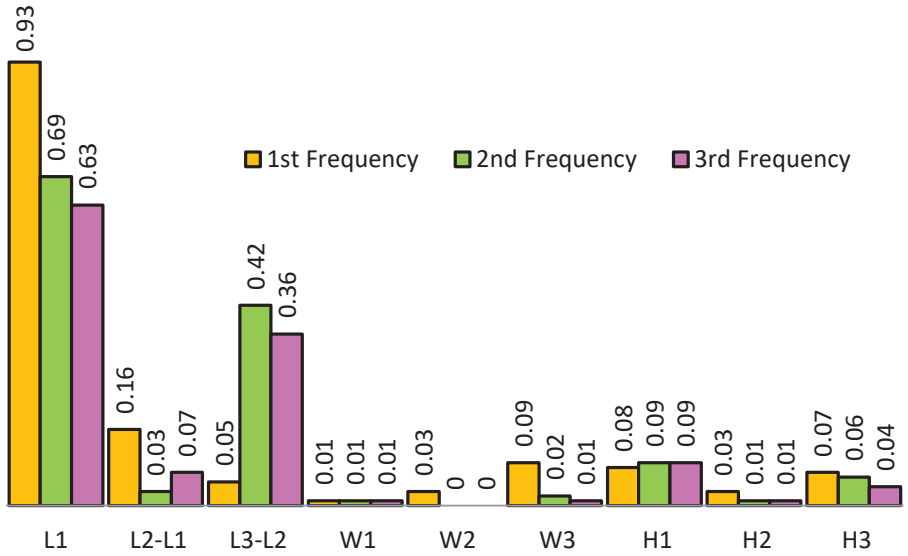

Fig. 20. Sensitivity percentage of geometric parameters on the first three resonance frequency

Figure (21) displays the results of investigating the effect of geometric parameters on the vibration amplitude in the first to third modes. According to this figure, the length of the first part of the MC, signified by L_1, had the maximum effect on the natural frequencies.

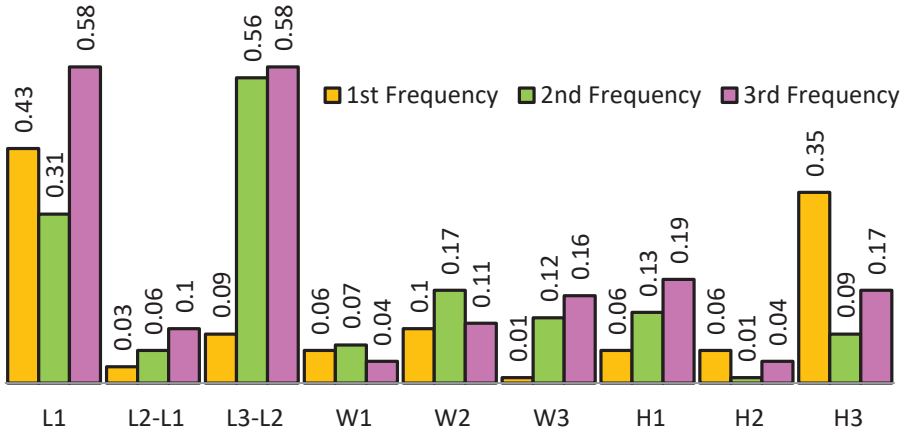

Fig. 21. Sensitivity percentage of geometric parameters on the first three MC amplitude

7. Conclusion

The present study intended to simulate AFM piezoelectric MC based on Timoshenko beam model and MCS theory. The equations were discretized based on the DQ method. Due to the lack of the experimental tests on the DMASP micro cantilever vibration behavior, the experimental tests including the measurement of the time and frequency response were performed in different moisture contents in near and far from the sample surface have been

investigated. Furthermore, the standard topography was compared the experimental results indicating that MCS theory is more accurate to predict the vibration behavior of AFM MC in nanoscale. The effect of capillary force on the MC vibration amplitude was assessed with regard to the environmental conditions caused by relative moisture content and temperature. The results indicated the reduction of MC amplitude while increasing the relative moisture content of the air. Sensitivity analysis leads to a better understanding of the system and helped to identify the parameters that had less impact on the system behavior. Moreover, the accuracy and speed of equation solving increased by eliminating the less-effective parameters based on the sensitivity analysis.

References

[1] B. Wang, J. Zhao, and S. Zhou, "A micro scale Timoshenko beam model based on strain gradient elasticity theory," *Eur. J. Mech. - A/Solids*, vol. 29, no. 4, pp. 591–599, Jul. 2010.

[2] S. K. Park and X.-L. Gao, "Bernoulli–Euler beam model based on a modified couple stress theory," *J. Micromechanics Microengineering*, vol. 16, no. 11, pp. 2355–2359, Nov. 2006.

[3] M. Şimşek, "Dynamic analysis of an embedded microbeam carrying a moving microparticle based on the modified couple stress theory," *Int. J. Eng. Sci.*, 2010.

[4] R. Ansari, M. Ashrafi, and S. Hosseinzadeh, "Vibration characteristics of piezoelectric microbeams based on the modified couple stress theory," *Shock Vib.*, 2014.

[5] J. N. Reddy, "Microstructure-dependent couple stress theories of functionally graded beams," *J. Mech. Phys. Solids*, vol. 59, no. 11, pp. 2382–2399, 2011.

[6] S. Kong, S. Zhou, Z. Nie, and K. Wang, "The size-dependent natural frequency of Bernoulli–Euler micro-beams," *Int. J. Eng. Sci.*, vol. 46, no. 5, pp. 427–437, May 2008.

[7] R.-F. Fung and S.-C. Huang, "Dynamic Modeling and Vibration Analysis of the Atomic Force Microscope," *J. Vib. Acoust.*, vol. 123, no. 4, p. 502, 2001.

[8] S. Mahmoodi, M. Daqaq, and N. Jalili, "On the nonlinear-flexural response of piezoelectrically driven microcantilever sensors," *Sensors Actuators A Phys.*, 2009.

[9] S. Nima Mahmoodi and N. Jalili, "Non-linear vibrations and frequency response analysis of piezoelectrically driven microcantilevers," *Int. J. Non. Linear. Mech.*, vol. 42, no. 4, pp. 577–587, May 2007.

[10] K. Wolf and O. Gottlieb, "Nonlinear dynamics of a noncontacting atomic force microscope cantilever actuated by a piezoelectric layer," *J. Appl. Phys.*, 2002.

[11] A. Korayem and M. Korayem, "The effect of surface roughness on the vibration behavior of AFM piezoelectric MC in the vicinity of sample surface in air environment based on MCS theory," *Precis. Eng.*, 2016.

[12] A. H. Korayem, A. Mashhadian, and M. H. Korayem, "European Journal of Mechanics A / Solids Vibration analysis of different AFM cantilever with a piezoelectric layer in the vicinity of rough surfaces," *Eur. J. Mech. / A Solids*, vol. 65, pp. 313–323, 2017.

[13] M. Damircheli and M. H. Korayem, "Sensitivity of higher mode of rectangular atomic force microscope to surface stiffness in air environment," *Micro & Nano Lett.*, vol. 8, no. 12, pp. 877–881, Dec. 2013.

[14] Y. Song and B. Bhushan, "Finite-element vibration analysis of tapping-mode atomic force microscopy in liquid," *Ultramicroscopy*, 2007.

[15] A. Kovacs and Z. Vízváry, "Structural parameter sensitivity analysis of cantilever-and bridge-type accelerometers," *Sensors Actuators A Phys.*, 2001.

[16] H. Lee and W. Chang, "Sensitivity of V-shaped atomic force microscope cantilevers based on a modified couple stress theory," *Microelectron. Eng.*, 2011.

[17] H. Korayem and R. Ghaderi, "Sensitivity analysis of nonlinear vibration of AFM piezoelectric microcantilever in liquid," *Int. J. Mech. Mater.*, 2014.

[18] M. H. Korayem, A. H. Korayem, and S. Hosseini Hashemi, "Analysis of hysteresis effect on the vibration motion of a bimodal non-uniform micro-cantilever using MCS theory," *Appl. Phys. A*, vol. 122, no. 2, p. 96, Feb. 2016.

[19] J. Katainen, M. Paajanen, E. Ahtola, and V. Pore, "Adhesion as an interplay between particle size and surface roughness," *J. Colloid*, 2006.

[20] M. Korayem and A. Korayem, "The effect of surfaces type on vibration behavior of piezoelectric micro-cantilever close to sample surface in a humid environment based on MCS theory," *Appl. Phys. A*, 2016.